

INTRODUCTION

Even with the surge in use of renewable energy, for the foreseeable future the primary energy source for power applications is likely to be fossil fuels, particularly with the low price of natural gas. Using these resources as efficiently as possible for both economic reasons and to minimize carbon dioxide emissions is critical (Viswanathan and Bakker, 2000; Viswanathan et al., 2005). In order for power plants to be more efficient they need to run at higher temperature: an operating temperature increase from 873 K to 1073 K would increase the efficiency from <40% to >50%, and reduce CO₂ emissions by 40-50% (Smith and Shoemaker, 2004). This requires materials that are strong enough, can withstand an environment that may contain impurities in addition to steam, display good oxidation and corrosion resistance and are economically viable (Viswanathan et al., 2005). The Department of Energy-defined goal for alloys for the next-generation Advanced Ultra Supercritical (AUSC) steam plants is 35 MPa at 1033 K, which are the conditions that we will focus on in this proposal. Affordable materials that can satisfy these requirements will also likely find use in supercritical CO₂ cycles and in tubing for concentrated thermal solar power.

The martensitic/ferritic alloys that are currently used in power plants are limited to operating temperatures \leq 873 K (Viswanathan and Bakker, 2000). Nickel-based superalloys, some titanium alloys, and, possibly, oxide-dispersion strengthened ferritic alloys (Miller et al., 2003, 2005) can satisfy the strength and, at least for nickel-based alloys, the oxidation and corrosion requirements at elevated temperatures. Unfortunately, these materials are too expensive except for use in specialized applications (Takeyama, 2007). This critical need for advanced materials for steam turbine components in ultra supercritical power plants has been long recognized and is the basis of efforts in Japan, Europe, China, India and the U.S. (Viswanathan and Bakker 2000; Takeyama, 2007, Di Gianfrancesco, 2017).

Recent efforts in this area have focused on devising new austenitic steels strengthened with Laves phases (Maziasz, 1989; Takeyama et al., 2001; Takeyama, 2007; Yamamoto et al., 2007a, 2007b, 2008), whose purpose is to provide a “grain boundary (GB) precipitation strengthening mechanism” (Tarigan et al., 2011, 2012). The addition of aluminum can be used to improve oxidation resistance in these alloys (Yamamoto et al., 2005, 2007a, 2007b; Brady et al., 2005, 2007a, 2007b). Such alumina-forming austenitic (AFA) stainless steels have shown promise to decrease our reliance on expensive nickel-base alloys for aggressive conditions in energy production and chemical processing environments (Brady et al., 2014). AFAs use alumina instead of chromia as a protective oxide scale for high corrosion resistance since it is known to offer even better protection at high temperatures (Kofstas, 1995; Heubner 2000). AFA stainless steels were in development as early as the 1970s (McGurty, 1978) and, more recently, a new family of AFAs has been under development at the Oak Ridge National Laboratory, ORNL (Yamamoto et al., 2005, 2007a, 2007b, 2008, 2011; Brady et al., 2005, 2007a, 2008; 2014). In the newer grades of AFAs, B2-structured NiAl and Laves phase precipitates are present on both the GBs and in the austenitic matrix, while MC precipitates or L1₂-structured Ni₃Al precipitates, which are present only in the matrix, are used to increase the creep strength (Brady et al., 2014; Yamamoto et al., 2008; 2011). While great strides have been made in the properties of these AFA stainless steels, optimization of their creep strength and oxidation resistance with a balance of cost for future commercialization (Brady et al., 2014) has been difficult because the deformation behavior is poorly understood.

This proposal is focused on the deformation behavior of these materials with an emphasis on elucidating the “grain boundary (GB) precipitation strengthening mechanism” (Tarigan et al., 2011, 2012). It will involve meticulous microstructural and defect characterization of the model AFA stainless steel Fe-20Cr-30Ni-2Nb-5Al before and after mechanical testing using both a transmission electron microscope (TEM) and a scanning electron microscope (SEM). *In-situ* straining studies will be performed in both a TEM and a SEM in order to elucidate both dislocation/precipitate and dislocation/GB interactions, including determining the role of the precipitate free zone present along the GBs. While most work will be performed at Dartmouth, TEM *in-situ* straining will also be performed at Brookhaven National Laboratory (BNL) through collaboration with Dr. Eric Stach, Group Leader, Electron Microscopy.

FURTHER BACKGROUND

Laves-Phase Strengthened Austenitic Stainless Steels

Takeyama et al. (2001) systematically studied Laves phase precipitation in the austenitic Fe-20Cr-(25-40)Ni-2Nb (in at. %) quaternary alloy system. The precipitates, which adopt the hexagonal C14 structure, are often referred to as the e phase. For alloys containing 35 at. % Ni, the precipitates are elongated with many interfacial dislocations, whereas for alloys containing 25 at. % Ni the precipitates are smaller and more equi-axed. In these Fe-Cr-Ni-Nb alloys, the *c/a* ratio of the precipitates decreases as the Ni content decreases for 15-25 at. % Ni and changes little with further increases in Ni content. At 25 at. % Ni the *c/a* ratio is about the same as that of binary stoichiometric

Fe_2Nb at 1.63, which is near the value for the cubic symmetry C15 Laves structure. Although the precipitates are referred to by Takeyama (2007) as Fe_2Nb , they contain 14-15 at. % Cr, 26 at. % Nb and 17-25 at. % Ni, depending on the overall alloy composition. Takeyama (2007) determined TTT curves for the precipitates and found that precipitation at 1173-1273 K occurred first on the grain GBs after ~ 300 s, but only after >1000 s in the matrix. After long ageing times (4.32×10^6 s, i.e. 1,200 h) the precipitates on the GBs became significantly larger ($\leq 3 \mu\text{m}$).

In contrast, Yamamoto et al. (2007b) found that the e Laves phase precipitates in the *matrix* of the alloy Fe-15Cr-20Ni-(1-2)Nb were relatively stable during both ageing and creep testing at 1073 K. This stability may arise partly from the semi-coherent interface of the Fe_2Nb precipitates, as indicated by the strain contrast present in TEM images even after long-term annealing (Takeyama, 2007), and also from the presence of small additions of Al, Mo, C and B. Small elemental additions have also been shown to stabilize Laves phases in other systems: Maziasz (1989) noted that Si additions led to the formation of $\text{Fe}_2(\text{Mo},\text{Nb})$ precipitates in austenitic alloys, while Yamamoto et al. (2008) found that small Zr additions promote Fe_2Ti Laves phase precipitates.

Yamamoto et al. (2008) studied the microstructural evolution of Fe-20Cr-30Ni-2Nb alloys with and without additions of 0.4 Si, 0.2 Zr or 5.0 Al (in at. %) during creep at 1023 K and 100 MPa. The Si addition helped to both refine the particle size (from $\sim 1 \mu\text{m}$ to 300 nm) and produce a greater volume fraction of particles during ageing at 1073 K, and stabilized them against coarsening, resulting in superior creep resistance. Interestingly, alloys that were only *solution treated* showed superior creep properties to those that were *aged* prior to creep testing. The authors speculated that this phenomenon was because the particles that were dynamically precipitated during creep were finer (300-400 nm) and, thus, more effective at pinning dislocations. The Zr addition improved the creep resistance more dramatically than the Si additions possibly by stabilizing very fine d- Ni_3Nb particles. The addition of Al not only improved the creep resistance due to the formation of 30 nm diameter Ni_3Al precipitates, but also improved the oxidation through the formation of a protective alumina layer on the surface.

The fundamental issues with the use of austenitic alloys for high temperature applications were clearly articulated by Yamamoto et al. (2008) who noted that “The strengthening effect of Fe_2Nb (Laves phase) strongly depends on its size and volume fraction, indicating that the thermal stability of the particle size and distributions is the key to improve creep properties.” More specifically, the two key issues are that: 1) the increase in size and density of the large Laves phase particles that develop on the GBs during creep testing (Yamamoto et al. 2008) will ultimately result in specimen failure when the GB coverage of these brittle particles is large enough; and 2) further refinement of the Laves phase precipitates to ~ 100 nm dia. is necessary to improve the creep strength (Yamamoto et al., 2008).

Tarigan et al. (2011, 2012) examined the effect of boron (0.03%) on the creep strength of Fe-20Cr-30Ni-2Nb (in at. %). Both the boron-doped and boron-free alloys contained Ni_3Nb precipitates (the g” phase at short annealing times and the d phase at long times) within the grains and Laves phase precipitates on the GBs. The boron decreased the creep rate and increased the creep rupture life by a factor of almost four. The role of boron appeared to be to increase the extent of the Laves phase precipitation at the GBs. Simply aging the *boron-free* alloy to increase the extent of GB coverage by the Laves phase from 52% to 89% also increased the creep rupture life, and decreased the creep rate to a similar extent as the boron addition. That even with 89% GB coverage by the Laves phase precipitates a creep rupture strain of 77% was attained shows that the precipitates do not necessarily embrittle the alloy. Tarigan et al. (2011, 2012) found that the creep rate, $\dot{\varepsilon}$, was related to the area fraction covered by the GB Laves phase, r, according to:

$$\dot{\varepsilon} / \dot{\varepsilon}_0 = (1 - r) \quad - (1)$$

where $\dot{\varepsilon}_0$ is the creep rate when $r = 0$. This idea is similar to earlier observations that in a Ni-20Cr-20W alloy the minimum creep rate decreased linearly with increasing density of an intergranular a_2 phase (Matsuo et al., 1987), and that increasing GB carbide precipitation in Ni-20 Cr and Fe-15Cr-25 Ni alloys increased their creep resistance (Zhang et al., 1987, 1989a, 1989b, 1991). Tarigan et al. (2011, 2012) suggested that the role of the GB phase was to suppress deformation at the GBs, whereas Zhang et al.’s (1989a, 1991) TEM observations suggested that the GB precipitation was associated with higher dislocation densities that strengthened the GB region.

Recently, Chen et al. (2014) also studied Fe-20Cr-30Ni-2Nb with and without 0.03% B and found that boron both increased the extent of and produced finer Laves phase precipitates on the GBs, but by <10% after their longest anneal of 24 h, when the GB coverage in the B-doped alloy was $\sim 80\%$. Using an EPMA, they showed strong boron segregation to the GBs. They found that for both the boron-doped and boron-free alloy, longer aging times prior to creep testing increased the creep life (by up to 100% for a 4 h versus a 12 h anneal), and that for the same aging time boron doping increased the creep life (by up to 44% for short aging times but by less at long aging times) by producing greater GB coverage of the Laves phase. Chen et al.’s (2014) results were very similar to those of Tarigan et al. (2011, 2012). Boron’s role appears to be to reduce the annealing time to obtain a large GB coverage

by the Laves phase.

Alumina-Forming Austenitic Stainless Steels

Even within particular grades of AFAs, the influence of specific precipitates on creep strength is complex. A wide variety of creep strengths can be obtained with relatively small changes in alloying elements, and phases that are beneficial in some AFAs appear to cause decreased creep strength in others. There are three grades of AFAs that have been investigated by the ORNL group based on their nickel content (in wt. %), *viz.*, 12Ni, 20-25Ni and 32Ni. The 12Ni grade alloys substitute Mn for some of the Ni both to stabilize the austenite relative to the deleterious d-Fe phase and to lower the cost. Unfortunately, this grade has been shown to have relatively poor creep resistance although the reason for the decreased creep strength is poorly understood (Brady et al., 2014; Yamamoto et al., 2011). In 20-25 Ni grade alloys it has been found that the total weight fraction of carbide phases is important. For example, in a 20-25Ni grade alloy with 2.53 wt. % Nb and 0.2 wt. % C there was little MC supersaturation and it showed poor creep resistance compared to 25Ni grade alloys with 1 wt.% Nb and 0.1 wt. % C. It is believed that the 2.53 wt.% Nb alloy showed poorer creep strength because the 2.53 wt.% Nb addition decreased the supersaturation of MC carbides (Brady et al., 2014). The 1 wt. % Nb and 0.1 wt. % C additions have been shown to be the optimal amounts for MC carbide strengthening in other studies of AFAs as well (Brady et al., 2008; Yamamoto et al., 2009). While increasing the Nb content from 1 wt. % to 2.5 wt. % seemed to have a detrimental role on the creep strength for a 25Ni alloy, in the 32Ni grade alloys with 3.3 wt. % Nb superior creep strength has been observed at 923 K, a feature that appears to be due to strengthening from $L1_2$ Ni_3Al precipitates, producing a creep strength almost five times greater than the best carbide-strengthened 20-25 Ni alloy. While the $L1_2$ Ni_3Al improved the creep properties of the 32Ni alloy, at 923 K it is believed that the metastable $L1_2$ Ni_3Al caused the decreased rupture time observed in a 25Ni-4Al-1Nb alloy with increased C content compared to a 25Ni-3Al-1Nb alloy. Although the creep strength was promising there was a tradeoff with significantly reduced creep elongation in the 32Ni grade alloy, which is thought to be due to σ -phase formation. At 1023 K, the 32Ni alloy creep results were comparable to those of both the 20-25Ni and 12Ni alloy grades (Brady et al., 2014).

Similarly, Dong et al. (2013) studied the creep behavior of Fe-19.95Ni-14.19Cr-2.25Al-2.26Mo-1.95Mn-0.15Si-0.01B (wt.%) at 973 K and 150 MPa and found that an alloy with 0.86 % Nb and 0.07 % C had poor creep behavior due to the relatively coarse (100 nm) NbC, whereas a similar alloy with a lower carbon content (0.04 %) had much smaller carbides (10 nm) and much improved creep properties. An alloy with the same carbon content but lower Nb (0.5%) and the addition of 0.2% V had even better creep properties due to the formation of (Nb,V)C. Both Laves phase and NiAl were found to be present after the creep testing, but Dong et al. (2013) questioned whether they contributed to the creep strength.

32Ni grade alloys with decreased chromium content (14 wt. % versus 19 wt. %) and additional alloying elements such as Zr and Ti have less σ -phase formation and improved creep properties. Indeed, a Zr, Ti alloyed 32Ni alloy with additions of carbon and boron was shown to have a creep-rupture life that exceeded that of the commercially-available Fe-base alloy A286 by an order of magnitude (Yamamoto, Muralidharan and Brady, 2013). Boron improves the creep properties of AFA stainless steels, but the underlying mechanism is unknown. Unlike the Al-free Fe-20Cr-30Ni-2Nb alloy studied by both Tarigan et al. (2011, 2012) and Chen et al. (2014), the addition of boron to a 32Ni grade alloy did not seem to have a significant effect on GB precipitation, and in this case it was hypothesized that the boron addition formed a strain field in the matrix that increased resistance to creep deformation (Yamamoto, Muralidharan and Brady, 2013). It is worth noting that unlike the Al-free alloys in which a solutionizing anneal can completely dissolve the Laves phase precipitates, in the more complex alloys developed at ORNL solutionizing anneals still leave substantial volume fractions of the Laves phase in the material (Yamamoto, Muralidharan, Brady, 2013; Brady et al., 2014, Hu et al., 2014).

While computational methods have helped in the design AFA alloys to limit the formation of deleterious phases, such as the sigma phase, and to help stabilize the austenitic matrix, it is clear that the additions of small alloying elements and their effect on the properties of AFA stainless steels require more detailed microstructural characterization. Even with an understanding of what phases may be present, creep mechanisms in this system are not well enough understood to predict which potential strengthening precipitate will be most beneficial for creep strength. For many of the AFA alloys that were also tensile tested, the creep and elevated temperature tensile properties did not correlate well. For example, in the 20-25 Ni grade alloys while B2-NiAl and Laves precipitation improves tensile properties, MC carbides appear to show a stronger influence on the creep strength (Brady et al., 2014; Yamamoto et al., 2011). The ORNL group also questioned whether the Laves phase even had any significant influence on the creep strength (Bei et al., 2010). The lower tensile strength they observed in these alloys at 1023 K compared to room temperature appeared to be due to the softening of the B2 NiAl phase which produces significant

strengthening at room temperature. This lack of correlation between the elevated temperature yield strength and the creep life is well illustrated in the data presented by Dong *et al.* (2013), see **Table 1**, although the strain hardening exponent, n , did show roughly the same trend as the creep life.

Table 1. Yield strength (YS), ultimate tensile strength (UTS), elongation to failure (e_f) and strain hardening exponent, n , of Fe-19.95Ni-14.19Cr-2.25Al-2.26Mo-1.95Mn-0.15Si-0.01B (wt.%) strained under tension at $7 \times 10^{-4} \text{ s}^{-1}$ at 1023 K, and corresponding creep life at 973 K and 150 MPa for various alloying additions. After Dong *et al.* (2013).

Alloying additions	YS (MPa)	UTS (MPa)	e_f (%)	n	Creep Life (h)
0.86 Nb, 0.07 C	229	272	50	0.109	164
0.86 Nb, 0.04 C	175	315	44	0.380	1002
0.50 Nb, 0.04 C, 0.20 V	160	330	52	0.479	1537

There has been little examination of the microstructure of specimens to failure. However, a recent study of the ORNL alloy DAFA 29 (Fe-14Cr-0.1Mn-32Ni-0.1Cu-3Al-0.2Si-2.9Nb-2Ti-0.1Mo-0.3Zr-0.1C-0.1B) showed that creep failure after 5282 h under a stress of 100 MPa at 1023 K showed cracking around the GBs with some cracks passing through precipitates and others circumventing precipitates. It is worth noting that it is unclear whether the crack path is exactly along the GB or whether it is really through the large precipitate free zone (PFZ) that is next to the GB. Also, the imposed stress was three times the “design” stress for these alloys.

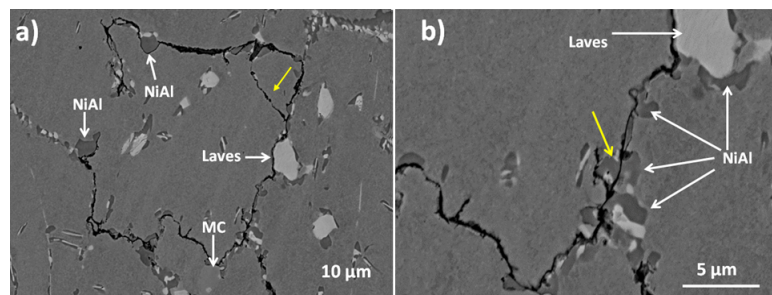


Figure 1. Backscattered electron images of a cross-section of DAFA stainless steel creep failure sample after a 1023 K/100 MPa test for 5282 h, (a) cracks on GBs, (b) higher magnification image of (a). From Hu *et al.* (2016b).

Results from Prior NSF Support:

DMR-1206240; Understanding Precipitation and the Mechanical Properties of Novel Laves Phase-Strengthened Austenitic Steels for Energy Applications; P.I. – I. Baker; 9/1/12-8/31/15; \$456,162.00.

The Intellectual Merit of this Activity was to understand both the effects of deformation on the precipitation processes in Laves phase-strengthened austenitic steels, including determining the mechanism of NiAl co-precipitation, and how these two kinds of precipitates affect subsequent *room-temperature* deformation processes. In addition, some preliminary creep testing was performed on two home-built constant-stress creep rigs, based on a design by Garofalo, Richmond and Domis (1962).

The Broader Impacts of the Activity include the education of a female African-American Ph.D. student, Geneva Trotter (now employed at Applied Predictive Technologies), a female American M.S. student, Natalie Afonina, and eight undergraduates: Hughes Lee, Ryan Strain, Evan Schlick, Hailey Nicholson, Amaris De La Rosa-Morena (a minority student), Bingyue Wang, Yi (Annie) Sun and Reed Harder, with the four women undergraduates supported by Dartmouth’s Women in Science Program. The later two were co-authors on a journal paper.

Two observations in the work have broad applicability to alloy design in other systems: (1) cold work can lead to more rapid precipitation of a higher volume fraction of finer precipitates; and (2) even with almost complete coverage of the GBs by a brittle phase, extensive room temperature tensile ductility can still be achieved (see below). The work has been disseminated by the publication of six journal papers (Trotter *et al.*, 2014a; Trotter and Baker, 2015a,b; Hu *et al.*, 2013, 2015; Trotter *et al.*, 2016), a paper recently submitted to a journal (Hu *et al.*, 2016a), and through eleven conference presentations (Trotter, Rayner and Baker, 2012, 2013a, 2013b; Trotter *et al.* 2014b, 2014c; Hu, *et al.*,

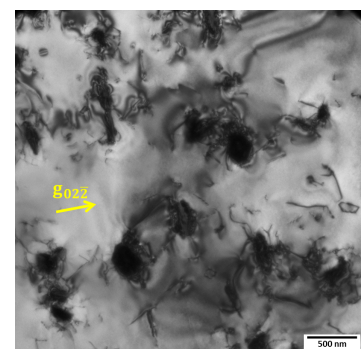


Figure 2. BF TEM image showing dislocations

punched out at Laves phase precipitates in Fe-20Cr-30Ni-2Nb-5Al aged for 2.4 h at 1073 K. After Trotter *et al.* (2014a)

2014; Trotter and Baker, 2015c, 2015d, 2016; Baker et al., 2016; 2017). The work involved collaborations with Drs. M.K. Miller and L. Yao (Oak Ridge National Laboratory), Drs. S. Chen and Z. Cai (Argonne National Laboratory) and Prof. P.R. Munroe (U. New South Wales, Australia).

Our work studied the effects of cold work on the simplified AFA stainless steel Fe-20Cr-30Ni-2Nb-5Al - many of the alloys studied by the ORNL Group and others are much more complex containing 10 or so elements (Brady et al., 2014). Cold rolling was performed, after solution treatment at 1523 K, to 25%, 50% and 90% rolling reductions with subsequent ageing performed for various times at 973 K, 1073 K and 1173 K. A significant density of dislocations was found in the matrix in the solutionized and aged specimens even without cold rolling, possibly due to the punching out of dislocations around the precipitates during cooling, see **Figure 2**.

We found that cold work accelerated the precipitation kinetics of both the C14-type Fe_2Nb -type Laves phase and the B2-type NiAl precipitates markedly compared to simply aging, presumably due to heterogeneous precipitation on dislocations, see **Figure 3**. It is worth noting that in the material that was simply aged, the Laves phase precipitates nucleate before the B2 precipitates, but it is no longer clear that this sequence occurs after cold work and aging, see **Figure 3**.

While often co-located, the Laves phase and B2 particles are distinct. L1_2 (ordered f.c.c.) precipitates were also present in samples aged at 973 K with 90% prior cold work, but not in specimens annealed at 1073 K, which is in line with thermodynamic calculations, see **Figure 4**. The additional fine L1_2 precipitates present at 973 K are presumably the reason for the greater hardness of the 973 K annealed material (Trotter et al., 2014a). We have shown, using atom probe tomography, that the L1_2 precipitates in the ORNL-developed AFA steel DAFA 26 are $\text{Ni}_3(\text{Al},\text{Ti})$. Compared to material that had not been strained, defects introduced by cold work not only caused more rapid precipitation in the matrix but also increased the total volume fraction of precipitates as compared to material that had been simply aged, see **Figure 3**. Histograms of the particle size distributions were produced for each annealing time and temperature (not shown here), and, as might be expected, they were

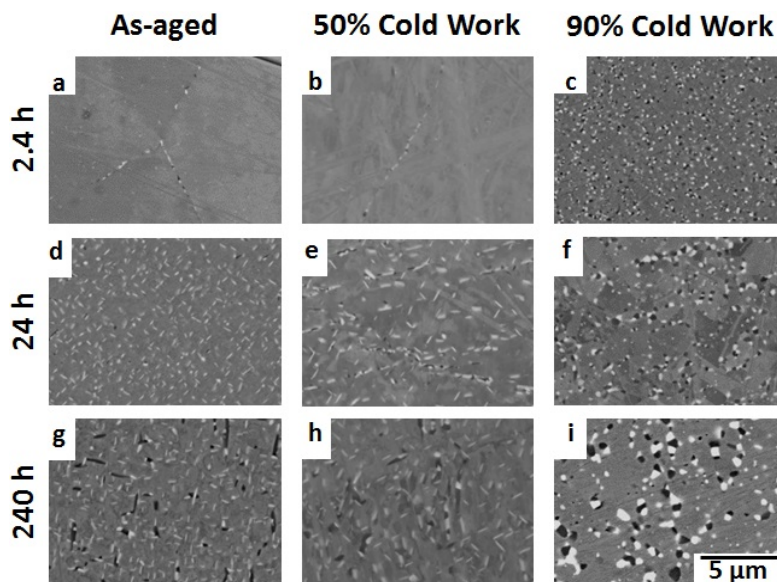


Figure 3. BSE images of specimens aged or cold rolled and aged at 1073 K for various times. Bright particles are the Laves phase; the dark particles are NiAl. From Trotter et al. (2014a).

The orientation relationship between the Laves phase precipitates and the austenite matrix was found to be $(0001)_{\text{Fe}_2\text{Nb}} \parallel (111)_\gamma$; $[10\bar{1}0]_{\text{Fe}_2\text{Nb}} \parallel [110]_\gamma$ (Denham and Silcock, 1969), while the B2 precipitates show the $(111)_m \parallel (011)_p$, $[\bar{1}01]_m \parallel [\bar{1}11]_p$ Kurjamov-Sachs relationship (Trotter and Baker, 2015a).

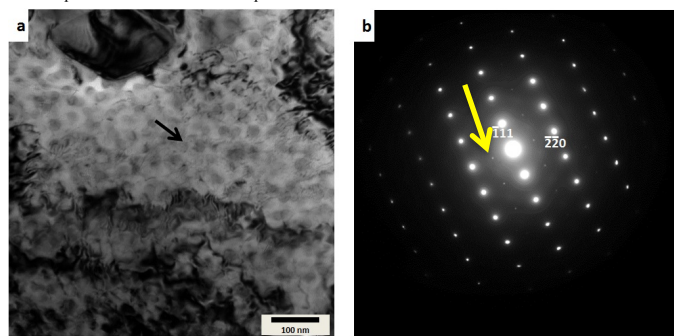


Figure 4. a) Bright field TEM image of Fe-20Cr-30Ni-2Nb-5Al after 90% rolling reduction and aged 240 h at 973 K; b) selected area diffraction pattern from area arrowed in a) showing L1_2 superlattice reflections (arrow points to a systematic row of L1_2 superlattice reflections). From Trotter et al. (2014a).

We also examined the effects of simply aging on the microstructure and room temperature tensile properties of

Fe-20Cr-30Ni-2Nb-5Al and the results are dramatic, see **Figure 5**. **Table 2** lists the average particle diameter for matrix and GB Laves and NiAl precipitates and the % GB coverage.

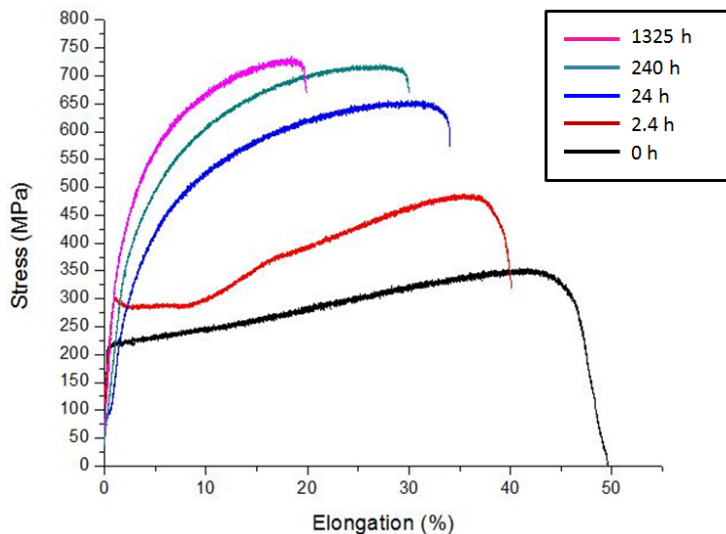


Figure 5. Representative tensile curves of Fe-20Cr-30Ni-2Nb-5Al homogenized at 1523 K for 24 h and aged at 1073 K for the different times indicated. Tensile tests were performed 3-4 times for each heat treatment. From Trotter, Baker and Munroe (2014).

After solutionizing for 24 h at 1523 K the Laves phase precipitates had dissolved, see **Figure 6**. This material had a yield strength of 205 MPa, an elongation to failure of 52% and a low, uniform work hardening rate of ~300 MPa. A 2.4 h anneal at 1073 K, which produced substantial GB coverage of fine alternating Laves phase and NiAl precipitates but only a few small precipitates within the grains, gave a 57% increase in yield strength to 322 MPa with an increase in work-hardening rate, and a slight reduction in elongation to 37%. For this heat-treatment *only* there is a clear yield drop and a long Lüders region, see **Figure 5**. Longer anneals increase the size and volume fraction of the precipitates both in the grain and on the GBs, and lead to almost complete coverage of the GBs after a 1325 h anneal, see **Figure 6**.

Table 2. Average particle diameter for matrix and GB Laves and NiAl precipitates for Fe-20Cr-30Ni-2Nb-5Al aged at 1073 K. From Trotter, Baker and Munroe (2014).

Aging time (h)	Laves (nm)		NiAl (nm)		GB Coverage (%)
	Matrix	GB	Matrix	GB	
2.4	95 ± 39*	192 ± 86	---	126 ± 75	56
24	205 ± 84*	332 ± 165	194 ± 103*	239 ± 124	78
240	252 ± 167*	335 ± 187	330 ± 149*	366 ± 187	84
1325	301 ± 170	743 ± 335	734 ± 668	864 ± 468	93

These changes increase the yield strength, work-hardening rate, and decrease the elongation, see **Figure 5**. The substantial increase in both yield strength and work-hardening rate for the longer anneals is consistent with Orowan looping around the precipitates within the grains, which produces substantial increases in dislocation density, including dislocation loops and dislocation dipoles. Remarkably, even though the GBs are completely covered in brittle NiAl and Laves phase precipitates after the 1325h anneal, the material can still show 19% elongation!

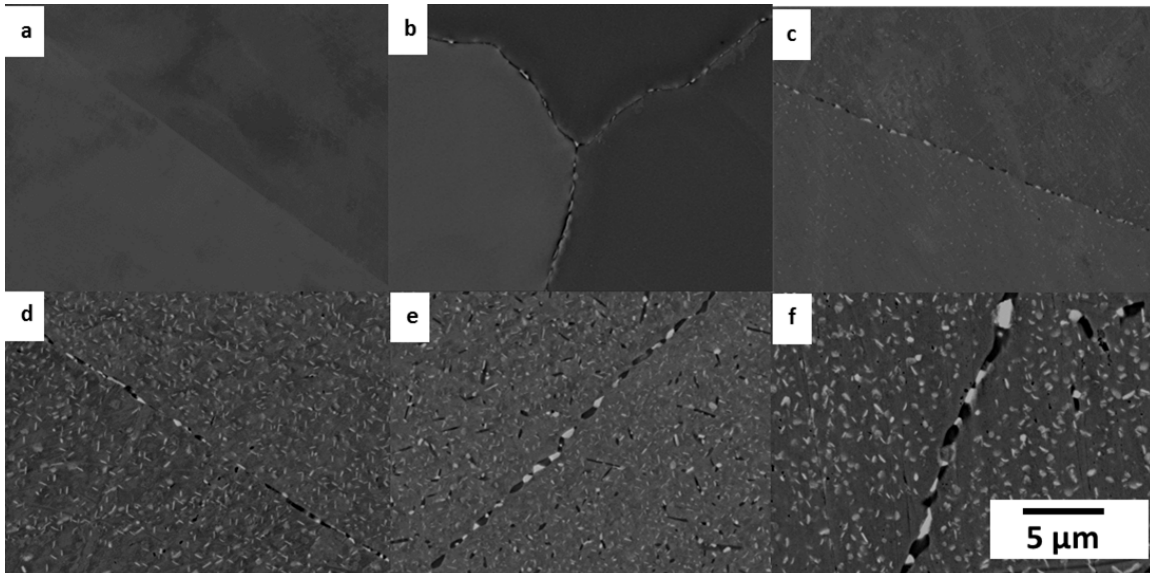


Figure 6. Backscattered electron images showing precipitation in Fe-20Cr-30Ni-2Nb-5Al: (a) after a homogenization anneal; and aged at 1073 K for b) 0.5 h, c) 2.4 h, d) 24 h, e) 240 h and f) 1325 h. Bright particles are the Laves phase; dark particles are NiAl. From Trotter, Baker and Munroe (2014).

Table 3. Yield strength (YS) and elongation to failure (e_f). From Trotter, Baker and Munroe (2014) and Afinona and Baker (2016). Results are the average of at least three tests at each condition.

Aging Time (h)	YS (MPa) 293 K	e_f (%) 293 K	YS (MPa) 1033 K	e_f (%) 1033 K
0	205	52	188	7.7
2.4	322	37	225	5.7
24	362	29	202	8.9
240	351	28	166	9.6
1325	383	19	N/A	N/A

We also performed tensile tests and preliminary creep studies at 1033 K on Fe-20Cr-30Ni-2Nb-5Al given four of the heat treatments (0, 2.4, 24 and 240 h at 1073 K) used for the room temperature tensile tests shown in **Figure 5**. In the 1033 K tensile tests the alloy exhibited significantly lower elongations than at room temperature for all ageing times, see **Table 3**, with no work-hardening observed. As might be expected, the yield strengths were lower at 1033 K compared to room temperature, but surprisingly the material annealed for 240 h, which was one of the strongest when tested at room temperature, was even weaker than the solutionized material. In fact, the latter material was only slightly weaker at 1033 K than at room temperature, possibly due to some very fine precipitation during the test.

Creep tests at 1033 K showed that the 2.4 h and 24 h annealed specimens had similar secondary creep rates, although the 24 h annealed specimen had a slightly larger creep strain due to the greater initial primary creep, see **Figure 7**. This result is, perhaps, a little surprising since the particle sizes were significantly larger and the GB coverage significantly greater for the 24 h-annealed specimen, and no NiAl was detected on the GBs for the 2.4 anneal. By comparison, the creep rate was significantly higher for the specimen annealed for 240 h, where particle sizes were larger still, but GB coverage was greater. Surprisingly, material tested in the solutionized condition (0 h anneal) shows a creep rate faster than that of the 2.4 h and 24 h annealed material, but much slower than the 240 h annealed material. As shown in **Figure 8**, precipitation occurred in the solutionized Fe-20Cr-30Ni-2Nb-5Al during creep testing, but this did not appear to affect the creep rate as testing continued. In fact, since the aging temperatures were only 40 K above the creep test temperatures, the precipitate structure examined in all the creep specimens had clearly evolved compared to the uncrept specimens, see **Figure 8**. We also examined the heads of the creep specimens, which had seen the same temperature but not the stress seen by the gauge of the specimens and the precipitate structure in these had evolved in a similar way to the gauge.

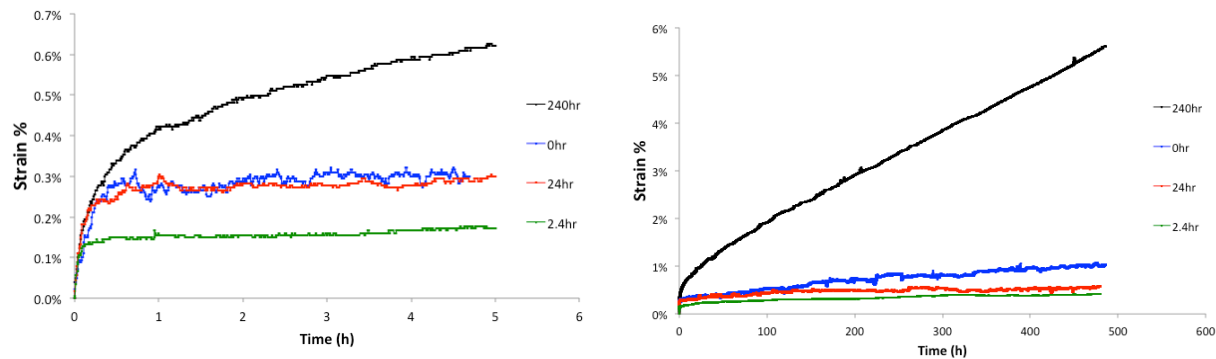


Figure 7. Creep curves for Fe-20Cr-30Ni-2Nb-5Al at 1033 K and 35 MPa for specimens aged for different times at 1073 K. Two tests were performed for each heat treatment. From Afonina and Baker (2016).

There are several interesting observations that can be made based on these preliminary creep studies. First, our results do *not* corroborate the observation made by others (Yamamoto et al. 2011; Dong et al., 2013; Brady et al., 2014) that the creep rate does not correlate well with the yield strength even if measured at the creep test temperature. The creep rates in **Figure 7** are clearly correlated with the yield strengths made at the same temperature (**Table 3**). Second, Yamamoto et al. (2008) found that solution-treated Fe-20Cr-30Ni-2Nb showed superior creep properties to those for material aged prior to creep testing, possibly because the particles that were dynamically precipitated during creep of the solution-treated material were finer. While the latter precipitation phenomenon certainly occurs in Fe-20Cr-30Ni-2Nb-5Al, this did not lead to a lower creep rate than in material given the shorter (2.4 h, 24 h) ageing anneals. Third, the results do not validate the empirical equation determined by Tarigan et al. (2011, 2012) and Chen et al. (2014) that the strain rate decreases with increasing coverage of the GBs by precipitates as shown in equation (1) since the 240-h heat treated material, which has the greatest GB precipitate coverage, shows a significantly higher creep rate than the 2.4 h and 24 h annealed material. A key difference from the work of Tarigan et al. (2011, 2012) and Chen et al. (2014) is that in their work the GB precipitates were *only* Laves phase (since their alloys did not contain Al), whereas the alloy tested here has alternating Laves phase and B2 precipitates, and the latter will likely be softer than the matrix at the test temperature. Fourth, the results also do not agree with the suggestion by Dong et al. (2013) and Bei et al. (2010) that the Laves phase and NiAl do not contribute to the creep strength since the 2.4 h- and 24 h-annealed Laves phase and NiAl particle-containing material have lower creep rates than the particle-free material.

Scientific Questions

The Results from Prior Research along with the reviewed literature suggest three intriguing questions:

1. How do gliding or climbing dislocations interact with the precipitates in austenitic AFA stainless steels both in the matrix and the GBs? In particular, how do the Laves, NiAl and Ni_3Al precipitates' size and spacing affect the creep strength of AFA stainless steels, and is the creep strength ultimately compromised by the PFZ?
2. How does the evolution of the precipitates under an applied stress at high temperature affect the deformation mechanisms?
3. How can an alloy in which brittle Laves and B2 phases almost completely cover the GBs still show good room-temperature tensile elongation (~19%)? Intimately connected to this is the role of the PFZ.

This proposal focuses on answering these questions. The answers will not only provide the relevant understanding to develop improved AFA stainless steels, but will also be useful for other advanced alloys that are being developed which incorporate brittle intermetallics and GB strengthening phases that were often avoided in alloy design in the past. In other words, having obtained answers to these questions, can we utilize thermo-mechanical treatments to optimize precipitate distribution and the size of the PFZ in AFA steels to improve their mechanical properties?

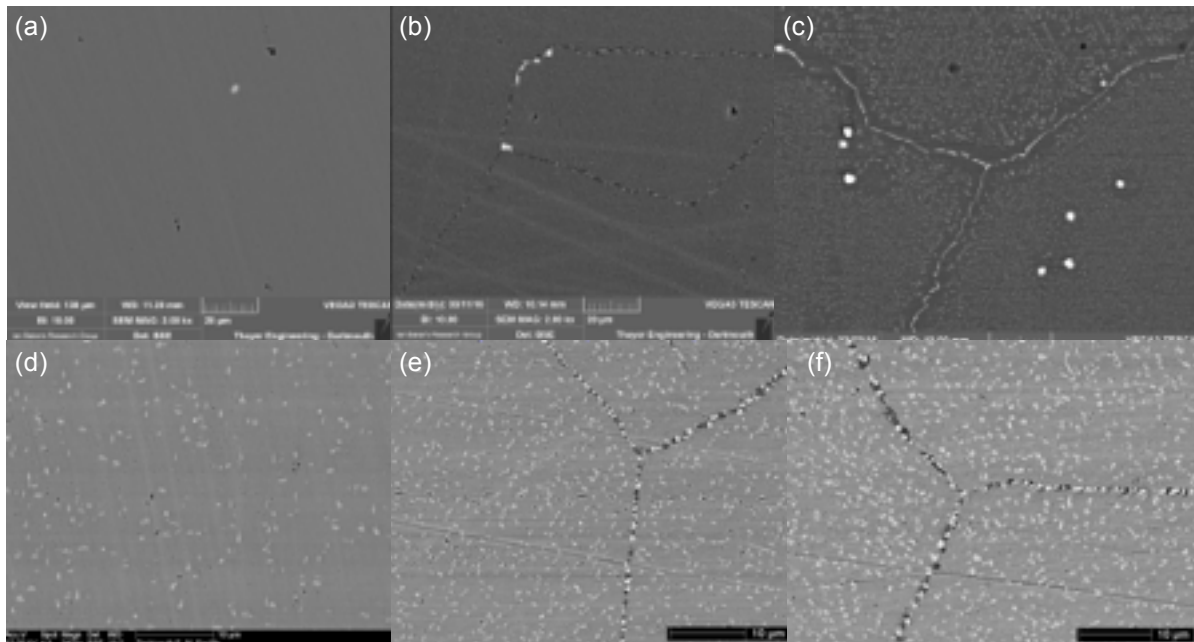


Figure 8. BSE images of Fe-20Cr-30Ni-2Nb-5Al (a) after homogenization anneal, (b) specimen in (a) post creep, (c) after 240 h at 1073 K, (d) after 24 h at 1073 K, (e) gauge and (f) head of specimen in (d) crept for 800 h at a stress of 35 MPa at 1033 K. The particles with light contrast are the Laves phase; the particles with dark contrast are NiAl. From Asonina and Baker (2016).

Intellectual Merit of the Proposed Activity

The aim and intellectual merit of the proposed activity is to ascertain the deformation mechanisms associated with GB precipitation strengthening, and to understand the fundamental deformation behavior in materials containing both a PFZ and multiple types of precipitates in both the GBs and the lattice each of which can contribute differently to the deformation behavior. The work will be performed on the model AFA stainless steel Fe-20Cr-30Ni-2Nb-5Al with which we have considerable experience.

PROPOSED RESEARCH

The research proposed here will attempt to elucidate the strengthening mechanisms in AFA stainless steels, and, in particular, we will attempt to answer the questions posed above.

Thus, we will:

1. Examine the dislocation structures in Fe-20Cr-30Ni-2Nb-5Al given different thermo-mechanical treatments and creep for different times.
2. Perform TEM *in-situ* straining experiments at room temperature and at 1033 K on both uncrept Fe-20Cr-30Ni-2Nb-5Al and material crept for different times.
3. Perform SEM *in-situ* straining experiments at room temperature and at 1033 K on both uncrept Fe-20Cr-30Ni-2Nb-5Al and material crept for different times.

Figure 9 is a schematic outlining the overall approach to the proposed work. We will use the same material as that previously used for the creep and high temperature tensile tests, i.e. a press-forged 8 kg ingot of Fe-20Cr-30Ni-2Nb-5Al supplied by Mr. Michael Schmidt, CarTech Corporation. The microstructure of the model alloy being studied is shown schematically in **Figure 10**.

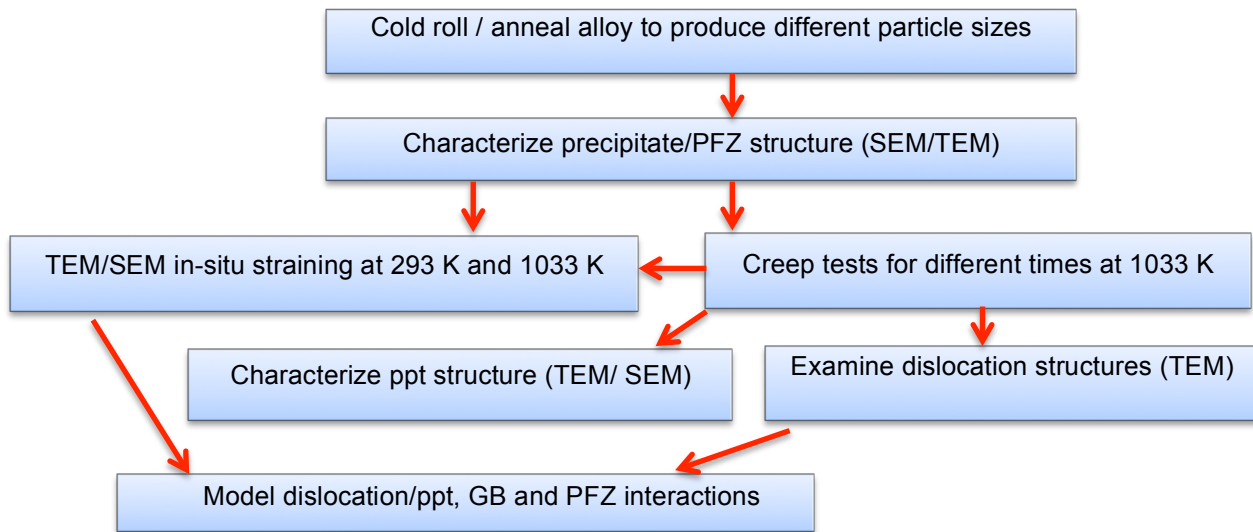


Figure 9. Schematic outlining the approach to the proposed work

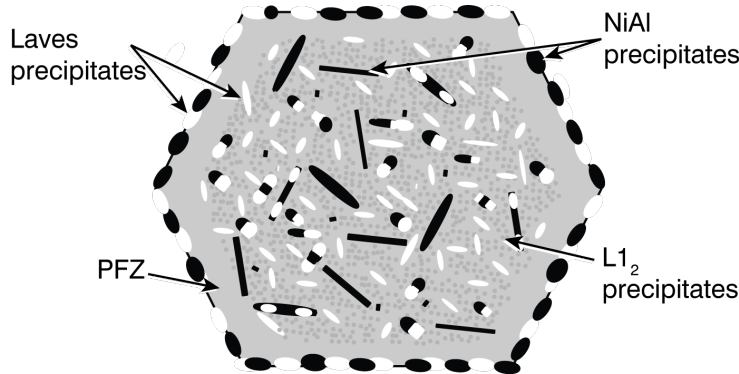


Figure 10: Schematic of the microstructure of a Laves phase-strengthened alumina-forming austenitic stainless steel. The f.c.c. matrix contains $L1_2$, B2 and Laves phase precipitates, while Laves phase precipitates and B2 precipitates also form along the GBs. A PFZ forms adjacent to the GBs at long annealing times.

There are three features to this structure:

1. *Matrix precipitates*: After elevated temperature annealing, the f.c.c. matrix contains fine coherent $L1_2$ Ni_3Al precipitates, and larger B2 NiAl and Fe_2Nb Laves phase precipitates. The Laves phase precipitates in the matrix nucleate before the B2 precipitates and, thus, for short annealing times it is possible to have only $L1_2$ and Fe_2Nb Laves phase precipitates in the matrix. All the precipitates coarsen upon annealing and the $L1_2$ precipitates may lose their coherency upon prolonged annealing.
2. *Grain Boundary precipitates*: Upon annealing the GBs become covered in B2 and Laves precipitates, whose size and extent increases with annealing time until almost complete GBs coverage occurs.
3. *PFZ*: At longer annealing times (240 h) a clear PFZ forms adjacent to the GBs. This region is potentially much weaker than the matrix and the GBs, and, thus, is a potential fracture path. On the other hand, the easier flow in the PFZ may allow it to accommodate strains from the GB.

Creep Tests

As noted above, we have already performed preliminary creep tests at 1033 K to 600 h for as-solutionized (0 h) Fe-20Cr-30Ni-2Nb-5Al and material annealed for 2.4 h, 24 h and 240 h at 1073 K. We will also perform constant-stress creep tests for shorter (100 h, 300 h) and longer times (1500 h, 3000 h or to failure) at 1033 K at a stress of 35 MPa. We have already loaded two specimens for the long-term creep tests, which will be ready for analysis should this proposal be funded.

To produce different amounts of GB coverage by the Laves phase and NiAl precipitates and different PFZ widths for similar precipitate distributions in the matrix, we will use two approaches. First, we will cold roll material before ageing at 1073 K. This accelerates precipitation in the matrix but not in the grain boundaries (Trotter et al., 2014a), see Figure 3. Second, we will age material at lower temperatures. This will lead to precipitation on

the GBs, but less so in the matrix. These additional specimens will allow us to separate effects associated with GB precipitation from effects due to matrix precipitation.

In monitoring the creep data, we will examine both the creep strain versus time (see, for example, **Figure 7**) and the creep strain rate versus creep strain. Analysis of the microstructures of specimens crept for different times (see below) will enable us to understand how the microstructure evolves over time and how this affects the creep behavior. These specimens will be used to make standard TEM and SEM specimens and TEM *in-situ* straining specimens,

Microstructural Analysis

Microstructural characterization of the alloys will be performed both *before* and *after* testing. It is worth noting that the head of the creep specimens provides material that has seen the same temperature and time, but has not seen the stress of the creep specimen gauge, and so this provides a specimen that has simply been annealed. Thus, we will compare specimens taken from the head with specimens taken from the gauge in order to understand what effect the applied stress has on precipitation (see **Figure 8**).

Backscattered electron imaging using a FEI XL30 field emission gun (FEG) SEM will be used to obtain the precipitate size distribution (frequency versus size) and spacing both within the grain and in the GB, as performed in Trotter et al. (2014a), see **Figures 3** and **6**. Diffraction-contrast transmission electron microscopy will be performed using a FEI Tecnai FEG 200 keV TEM to examine the precipitates in detail. A previous report on crept Laves-Phase-strengthened austenitic steels have suggested that the Laves phase precipitates become smaller during creep (Yamamoto et al., 2008). Both energy dispersive spectroscopy (EDS) and convergent beam electron diffraction (CBED) will also be performed to clearly identify the precipitates. Higher Order Lower Zone (HOLZ) line shifts in the transmitted disc in CBED patterns will be used to assess strains in the phases (Williams and Carter, 1996).

Deformation Mechanisms

Three approaches will be used to examine the deformation mechanisms.

Post-mortem TEM dislocation analysis will be performed on specimens crept at 1033 K and from room temperature tensile testing. Of particular interest is how changes in precipitate size and spacing affect the precipitate's interactions with dislocations and whether greater GB precipitation is associated with increased dislocation densities in the GB region, as reported by Zhang et al. (1989a, 1991).

Two *in-situ* straining approaches (*in-situ* TEM, *in-situ* SEM) will be performed at both room temperature and 1033 K in order to examine the deformation mechanisms for a variety of precipitate sizes and spacings (see above). We will also perform some TEM *in-situ* straining experiments on crept specimens.

TEM in-situ Straining: TEM *in-situ* straining experiments will be performed at both room temperature and 1033 K on Fe-20Cr-30Ni-2Nb-5Al with different particle sizes and spacings (see above) in order to observe the fundamental dislocation/precipitate interactions directly. It is worth noting that the P.I. has nearly 30 year's experience with TEM *in-situ* straining experiments (Baker, Horton and Schulson, 1987; Baker, Schulson and Horton, 1987; Baker, Guha and Horton, 1993; Baker, and Horton, 1993; Baker et al., 1991; Baker and Liu, 1994; Horton, Baker and Yoo, 1991; Nagpal and Baker, 1991; Nagpal, Baker and Horton, 1994; Loudis and Baker, 2008; Liao and Baker, 2008, 2011a, 2011b), including recent work by Liao and Baker (2011a, 2011b) where TEM *in situ* straining observations at various temperatures up to 900 K were used to quantitatively explain the yield stress anomaly observed in Fe₂MnAl.

Numerous features can be observed during TEM *in-situ* straining experiments including dislocation cross-slip, dislocation climb, dislocation pinning, and dislocation pile-ups. The curvature of dislocations can be used to estimate local stresses, e.g. Liao and Baker (2011a, 2011b), and the shift of HOLZ lines in the transmitted disc in CBED patterns will be used to assess local strains (Williams and Carter, 1996). TEM *in-situ* straining is not that useful for studying fracture per se since the fracture path in a thin foil may be different to that in the bulk (Baker, Horton and Schulson, 1987; Baker, Schulson and Horton, 1987).

SEM in-situ Straining: SEM *in-situ* straining experiments will be performed at both room temperature and 1033 K on Fe-20Cr-30Ni-2Nb-5Al with different particle sizes and spacings in attempts to examine the fracture path, i.e. does it occur through GB precipitates, between the precipitates and the PFZ, or through the PFZ: the path may change depending on the heat treatment. The experiments will be performed on notched specimens so that we know in advance approximately where fracture will occur. The specimens will be recorded continuously during *in-situ* straining, but they will also be examined post-straining at high resolution. In addition to BSE imaging of the

precipitates, electron channeling contrast imaging will be used to provide a view of the dislocation behavior after straining (Welsch et al., 2016).

Mechanisms

It is worth considering what may happen during *in-situ* straining of an AFA steel. In general, at room temperature dislocations will cut through small coherent deformable particles, and loop around larger nondeformable particles (Orowan looping). The former produces a low work-hardening rate since once the particle is cut by a dislocation, passage of subsequent dislocations is easier. Since the dislocation cuts the particle, the strength of the alloy is strongly dependent on the properties and dislocation behavior of the particle. For Orowan looping, the strength is strongly dependent on size and spacing but not on the mechanical properties of the particles. Examination of the stress-strain curves in **Figure 5** suggests that particle cutting may be occurring in the material annealed for 2.4 h since this exhibits a low work-hardening rate (although considerably higher than that of the unannealed, particle-free material). For longer annealing times, the substantially higher work-hardening rate suggest that Orowan looping is occurring, although one might expect the work-hardening rate to decrease with increasing annealing times as the particles increase in size and the interparticle spacing decreases.

While this simple picture of particle cutting versus Orowan looping is appropriate for a material with a single type of precipitate, it may not be appropriate for the AFA steel studied here, which has three different precipitates. The Laves phase is not likely to deform at room temperature, and in the ORNL alloy DAFA 29 very large Laves precipitates, which are formed during the casting process, crack during room temperature deformation, see **Figure 11**.

On the other hand, when the L_{12} precipitates are small, $a/2 [101]$ dislocations gliding on a $\{111\}$ slip plane will pile-up at the particle interface, and eventually glide through the precipitate in pairs of $a/2 [101]$ dislocations-coupled by an anti-phase boundary (APB) on $\{111\}$, see **Figure 12(a)**. This behavior occurs in some nickel-based superalloys and aluminum alloys containing L_{12} precipitates. It might also be possible for dislocation cutting to occur in the B2 particles. As noted earlier, the $(111)_m // (011)_p$, $[\bar{1}01]_m // [\bar{1}11]_p$ Kurdjumov-Sachs relationship was observed between the B2 particles and the f.c.c. matrix (Trotter and Baker, 2015a). Slip typically occurs by $a<010>$ or APB-coupled $a/2<111>$ dislocations at room temperature in B2 compounds (Baker, 1995), with NiAl-based B2 compounds normally deforming by the glide of $a<100>$ dislocations. The $a/2<111>$ dislocations gliding in the f.c.c. matrix might lead to $a<010>$ or APB-coupled $a/2<111>$ dislocations gliding in the B2 particles since the slip planes are aligned, see **Figure 12(b,c)**. As the L_{12} and B2 precipitates increase in size upon annealing, the deformation behavior will eventually change from dislocation cutting to Orowan looping. However, the particle size at which this transition occurs will be different for different types of particles since it depends on the surface energies on the slip planes, the Burger's vector and the shear modulus. For larger undeformable particles ($\geq 0.1 \mu\text{m}$), substantial local lattice rotations (up to $\sim 45^\circ$) occur around the particles at larger deformations (Humphreys 1979), the local lattice rotations increasing with increasing particle size for a given strain.

A priori, it is not clear whether dislocation looping or particle cutting occurs in the three different precipitates, at what particle size particle the transition from cutting to looping occurs, whether one type of particle controls the strength or all contribute to the strength. We should also note the observation in **Figure 2** that dislocations are punched out at the Laves phase particles due to the differences in thermal expansion between the particles and the matrix. This may mean that gliding matrix dislocations do not encounter the particles per se, but interact with the dislocations around the Laves phase particles.

Turning to high temperature deformation, at elevated temperature cutting and looping can still occur, but, dislocations can also climb around precipitates (Honeycombe, 1984) and cross-slip around the precipitates becomes more likely (Smallman, 1985). It is worth noting that if dislocation cutting of the precipitates occurs, this can lead to mechanical dissolution of the precipitates and at elevated temperatures their re-precipitation. In other words, there are a greater number of possibilities of how deformation takes place at higher temperatures.

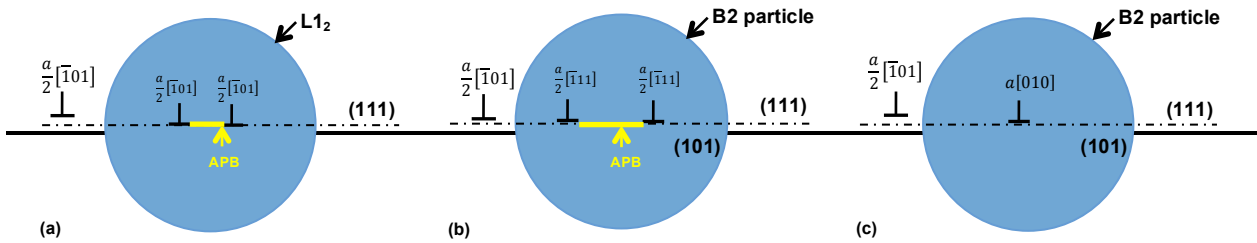
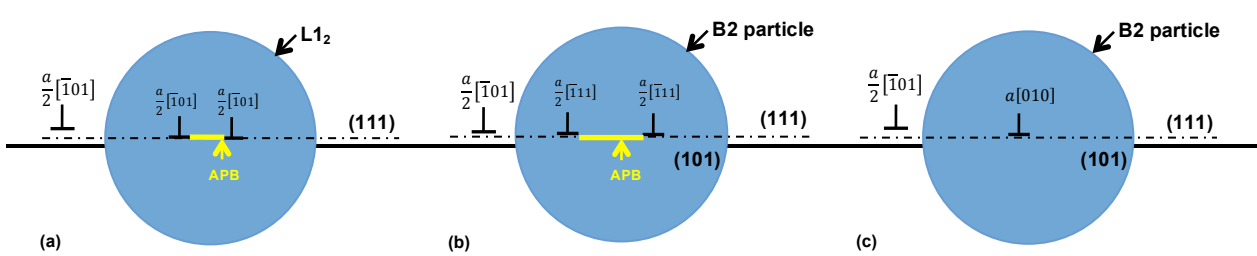


Figure 11. BSE image showing cracks (black features) in Laves phase precipitates in DAFA29 after straining at 293 K.



interaction of an $a/2<101>$ dislocation gliding on $\{111\}$ in an f.c.c. matrix with (a) an $L1_2$ precipitate in which slip is by $<111>$ dislocations on $\{101\}$, and (c) a B2 precipitate in which slip is by $<010>$ dislocations on $\{101\}$.

Regarding how this applies to the AFA steel, we do not know whether the $L1_2$ particles will get softer or harder with increasing temperatures as some $L1_2$ compounds such as Ni_3Al can show a yield anomaly (Pope and Ezz, 1984; Liu and Pope, 1995). In contrast, the B2 precipitates would be expected to lose their strength at $\sim 0.45 T_m$, where T_m is the melting point, as is observed in B2 alloys (Baker 1995). Laves phases are brittle but they can show plastic flow under compression even at room temperature via a twinning mechanism involving synchroshear though the movement of $1/6<211>$ synchroshockley partials on the basal plane (Chu and Pope, 1993a,b; Hazzledine and Pirouz, 1993; Kumar et al, 2000; Kumar and Hazzledine, 2004; Chisholm, Kumar and Hazzledine, 2005; Takata et al., 2009, 2013a, b, 2016; Heggen, Houben and Feuerbacher, 2010; Yang et al., 2012). Interestingly, Takata et al. (2013a) found both basal and non-basal slip occurred at a lower stress in Laves phase nanopillars, which had previously been nanoindented than in non-nanoindented nanopillars, suggesting that the difficulty of dislocation nucleation contributes to their normally brittle behavior. Chu and Pope (1993a,b) found plastic flow occurred at 1073 K, in a C15 Laves phase by $1/2<110>$ slip. Recent TEM observations of the ORNL alloy DAFA29 indicate that dislocation glide occurs within the Laves phase precipitates during straining at 973 K, see **Figure 12**.

The creep curves in **Figure 7** clearly indicate that the particles improve the creep rate, and that this improvement becomes less as the particles get bigger. A key question is do all the particles contribute to the improved creep rate or only some of them, and do the deformation mechanisms change as the particles get bigger. Also, can the B2 particles, which will be softer than the matrix, strengthen the material by trapping gliding matrix dislocations.

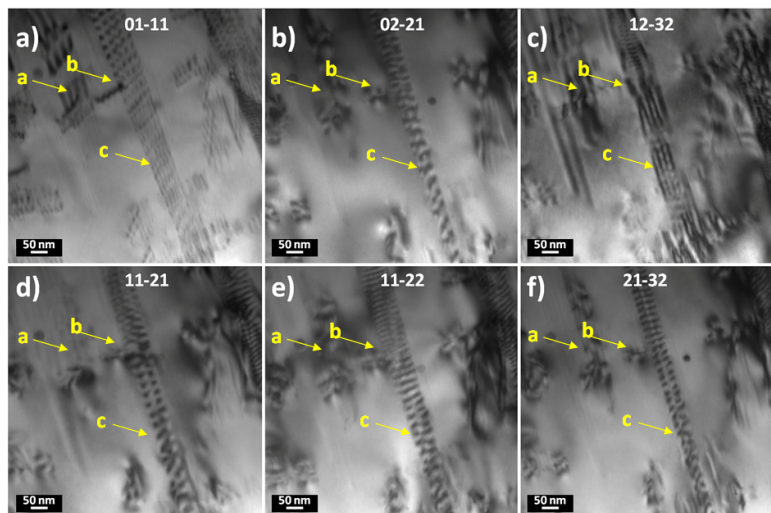


Figure 12. BF TEM images of dislocations and stacking faults in a Laves phase precipitate in DAFA29 tensile tested at 973 K at $5 \times 10^{-6} s^{-1}$. From Hu and Baker (2016).

densities that strengthened the GB region. Research on f.c.c./B2 lamellar structured FeNiMnAl alloys showed that initial yielding occurred in the softer f.c.c. phase, but that the B2 phase yielded once work hardening in the f.c.c. phase had increased its flow stress to the yield stress of the B2 phase (Liao and Baker, 2011). Also, for the shorter annealing time of 2.4 h only about half of the GB is covered in dislocations. How does this affect the deformation at the GBs?

During high temperature deformation, the GBs could be viewed quite differently. Now, there is a hard Laves phase precipitate and a soft B2 precipitate. Is this advantageous, or does deformation within the B2 particles cause strains at the GBs that cause the fracture. This would be consistent with the lower fracture strains observed in

Thus far, we have only discussed the behavior of particles in the matrix, however, the Laves phase and B2 phase particles were originally added to AFA steels as GB strengtheners. Thus, we will also examine the interaction of gliding dislocations with the B2 and Laves phase precipitates at the GBs. At room temperature, these phases are expected to be harder than the matrix and would be strong barriers to dislocation transmission. Of interest is whether dislocations impinging on the GB behave differently when they encounter a B2 precipitate rather than a Laves phase precipitate – as noted earlier, Tarigan et al. (2011, 2012) suggested that the role of the GB Laves phase was to suppress deformation at the GBs, whereas Zhang et al.'s (1989a, 1991) TEM observations suggested that the GB precipitation was associated with higher dislocation

tensile tests at 1033 K compared to room temperature, see **Table 3**. An alternative is that strains generated at the GBs lead to punching out of dislocations in the nearby matrix.

A further complication both for understanding both room temperature and elevated temperature deformation is the presence of a PFZ, which is quite pronounced in the AFA steel at longer annealing times. Nembach and co-workers (Bainter et al., 2003; Krol et al., 2003) used *in-situ* TEM straining to study the interaction of gliding dislocations with the PFZ in the polycrystalline gamma-prime strengthened nickel-based superalloy Nimonic PE16. They found that the PFZ reduces the yield strength only if the width of the PFZ's exceeds $1.7(l - r)$, where l is interparticle spacing and r is radius of the L_1 particles. For widths greater than this, dislocations are generated in the PFZ itself and the resulting dislocation pile-ups lead to a yield strength reduction. Thus, a question regarding the PFZ is whether this acts differently than the matrix, allowing significantly more strain there since it is softer than the matrix.

The TEM *in-situ* straining studies will be performed on Dartmouth's Tecnai FEG TEM for which the P.I. has a Gatan single-tilt, hot-straining stage (operates to 1273 K) and a video system. It is important to correlate the *in-situ* straining experiments with the post-mortem TEM analysis. The latter can provide Burgers vector information, but always has the possibility that the dislocations have rearranged themselves (particularly after high temperature deformation) so that one does not see the real line direction of the gliding dislocations. These studies will benefit from the utilization of a first-of-its-kind direct electron detector at BNL, which allows capture of *in-situ* videos at unprecedented time resolution, with full resolution data obtainable at up to 1600 frames/sec. BNL personnel also have considerable experience with TEM *in-situ* straining experiments. It is worth noting that while the macroscopic loading rates in both of these set-ups can be varied, control is not precise enough to determine strain rate sensitivities.

Analysis of the Results

Rösler and Artz (1990) developed a model to predict the creep rate for a particle-containing material. However, this is for a single type of hard undeformable, typically oxide, particle in which the rate controlling mechanism is breaking away from the particle after the dislocation has largely bypassed it (Schröder, and Arzt, 1985; Czyska-Filemonowicz et al., 1995; Häussler et al., 2001). The model does not consider GB particles. Zhang et al.'s (1991) creep model attempts to separate the strengthening from precipitates in the grain from those in the GB but again includes only one type of undeformable particle. Neither model incorporates the possibility that softer particles may strengthen the material. While the primary goal of the proposed work is not model development, we will attempt to develop a model based on our experimental observations. What form this will take is difficult to say. It is worth noting that the P.I. has experience in developing deformation models e.g. on the role of both GBs and particles on the ductility of intermetallic compounds (Baker and Schulson, 1989; Baker, 1999); a well-accepted model for the yield anomaly in FeAl (George and Baker, 1998); and a model for strain-induced ferromagnetism in intermetallic compounds (Yang, Baker and Martin, 1999; Wu, Munroe and Baker, 2003).

Personnel/Budget/Timeline

The project will run for three years with a starting date of September 1st, 2017. The P.I., a Ph.D. student and a number of undergraduates, typically two per year, will perform the work. Funds are requested for graduate student support, partial support of the P.I., travel, TEM/SEM time and supplies.

BROADER IMPACTS OF THE PROPOSED ACTIVITY

The results from this work will help to elucidate the deformation behavior of AFA stainless steels by understanding the interactions between dislocations and the precipitates. This will help not only in the future design of AFA steels but in understanding deformation in commercial alloys such as Crofer 22H (Barrilao, Kuhn and Wessel, 2016) and in several alloys being developed (Kuhn et al., 2016; Yamamoto et al, 2016; Takeyama, 2007; Tarigan et al., 2011, 2012) in which Laves phase precipitates are present in both the matrix and cover the grain boundaries and a PFZ is present. It will elucidate whether brittle GB precipitates are useful to incorporate in alloys for creep strengthening, and if the inclusion of precipitates that are softer than the matrix can improve creep behavior. It will attempt to understand why substantial tensile ductility is possible even when the GBs are covered with brittle phases, which will aid in their incorporation in other alloys systems. Finally, it will aid in designing and understanding the deformation behavior of novel alloys that contain multiple types of precipitates with different properties. The deliberate incorporation of brittle intermetallic compounds represents a paradigm shift in alloy design.

The project will also lead to the training of a number of undergraduates and a Ph.D. student.

Promoting graduate training: At the end of the project, in addition to the knowledge from formal coursework, the Ph.D. student will have gained skills in mechanical testing and materials characterization. For professional development, the student will take the Teaching Science seminar offered by Dartmouth's Center for the Advancement of Learning. All graduate students are required to undertake Dartmouth's Ethics training program. The P.I. will support and encourage the student to attend professional development workshops such as the Teaching Science seminar and the Communicating Research workshop series offered through Dartmouth's Center for the Advancement of Learning (DCAL), which was attended by the student on the current project. Dartmouth's Outreach Office works with DCAL to integrate these trainings with opportunities for hands-on application through science outreach in local schools, such as lunch-time Science Cafes where graduate students have informal conversations with middle school youngsters about their fields, and Science Pubs, in which community members and researchers have lively conversations about science topics. DCAL does formative assessments of its graduate student professional development programs for continuous quality improvement; outcomes of our Ph.D. program are assessed through both a Thayer School survey and an on-line survey for comparison with other institutions. Ph.D. students have an exit interview with the Assistant Dean for Academic Affairs.

Innovation: Thayer School of Engineering offers a Ph.D. Innovation Program designed to teach students the skills needed to be effective in the innovation process. Innovation Ph.D. fellowship funding is available after a student's 3rd year. We expect that the graduate on this project will join this program.

Integrating research and teaching: The P.I. expects to have two undergraduates assist on the project each year funded by NSF REU funds, Dartmouth's nationally honored Women in Science Project (WISP) and possibly a student (male or female) funded by the Thayer School's First Year Research in Engineering (FYRE) program that started in 2015. They will gain laboratory and research experience and will be required to take both laboratory safety and ethics training before starting their research. Typically, the PI has 5-6 undergraduates per year who work with graduate students on funded projects. They are typically supported by WISP, FYRE or by NSF REU funds. The Ph.D. student will share responsibility for mentoring the undergraduates, whose research on this project will integrate closely with their own. The undergraduates will take both laboratory safety and ethics training before beginning research. Minorities and, particularly, women have been well represented in amongst undergraduate participants.

Broadening participation: Dartmouth courts minority students at all degree levels, and we will encourage women and members of minority groups to apply for the graduate student position on this project. The Thayer School of Engineering at Dartmouth College will pay for the travel to Dartmouth of any suitable applicants. Currently 38% of Ph.D. students at Thayer School are female and 50% of the P.I.'s graduate students are women; at the undergraduate level 52% of 2016 graduated engineering majors at Dartmouth were female! The P.I. has a track record of successfully mentoring women students through participation in institutional programs such as Dartmouth's WISP program and will build on this experience (the PI has a fifteen-year WISP participation award). WISP, which has been successful in improving retention rates of women in science and engineering at Dartmouth, emphasizes student research experience. In addition to encouraging broader participation of women in science and engineering, this type of hands-on, interactive, contextual and collaborative learning has been shown to encourage participation of other underrepresented groups (Green et al. 2000; Goodman 2002; Lopatto, 2007; Hunter, Laursen and Seymour, 2007).

Broad dissemination: In addition to publishing the results of the research in refereed journals and presenting them at conferences, we will work with the Science Writer in Dartmouth's Office of Public Affairs to disseminate new findings on Dartmouth's web site and to the news media as appropriate. In addition, material developed in this work will be used in a graduate course on Materials Characterization.